

## A CHEMICAL/GAS PLUME TRACING ROBOT SIMULATOR FOR QUADROTOR PLATFORMS: A MODIFIED GAUSSIAN-MEANDERING PLUME PROPAGATION MODEL

*Kok Seng Eu<sup>1</sup>, Kian Meng Yap<sup>2</sup>*

<sup>1,2</sup>School of Science and Technology, Sunway University  
No. 5 Jalan Universiti, Bandar Sunway, 46150 Petaling Jaya  
Selangor, Malaysia

Email: <sup>1</sup>stevene@sunway.edu.my; <sup>2</sup>kmyap@sunway.edu.my

DOI: <https://doi.org/10.22452/mjcs.sp2019no1.1>

### ABSTRACT

*The process of evaluating the performance of chemical/gas plume tracing (CPT) algorithms is difficult because of real-world environmental parameters (i.e. surrounding wind) that are beyond researchers' control, therefore, a CPT simulator can be useful. In this study, we design a modified Gaussian-meandering plume propagation model that is enhanced with the realistic characteristics of plume propagation such as meandering, internal intermittency, and vortices, which have not been modelled in the previous studies before. Subsequently, we use a computational fluid dynamics (CFD) software to generate the three-dimensional (3D) wind vectors and study the impact of quadrotor's propellers, and then incorporating into the plume propagation design. On the whole, the study presented a complete CPT simulator for quadrotor platform with the realistic characteristics of plume propagation.*

**Keywords:** *Gas Dispersal Simulator, Chemical/Gas Plume Tracing, Robotics Olfaction, Gas Sensing, Quadrotor*

### 1.0 INTRODUCTION

Natural gas leak is a serious environmental disaster that is difficult to detect because natural gas is colorless and not visible to human eyes. As such, it will be hard to prevent gas leaking when they occur. A recent case was reported in California, United States, where 100,000 tons of methane gas was leaked into the atmosphere [1]. Such an incident can worsen global warming and eventually affect the climate system. Additionally, natural gas contains harmful chemicals and long-term exposure can cause health issues for residents living in the surrounding areas [2].

Autonomous quadrotors equipped with gas sensors can be programmed with algorithms to explore, track, and identify natural gas leaks. These could be a potential solution to the gas leakage problem [3]. However, there are still many challenges to overcome in order to apply autonomous quadrotors in the real world.

One of the main challenges is the design of chemical/gas plume tracing (CPT) algorithms. To overcome this, we can look to biological vectors for inspiration. For instance, a male moth employs a three-dimensional (3D) CPT technique by detecting and tracing pheromones from a female moth up to 11 km away. This CPT technique, which involves two strategies – surge and cast – has been studied by scientists. Moths employ the surge strategy whenever pheromones are detected; however, the plume of pheromones is nonlinear, turbulent, and chaotic. Eventually, the tracing of the plume will be lost. Hence, the casting strategy comes into play. The casting strategy is an orthogonal zigzag movement that slowly increases in oscillation amplitude until pheromones are detected. Subsequently, moths alternate between surge and cast strategies until the target source is found. Unfortunately, the moths' CPT technique cannot be completely applied to quadrotors as the flying mechanisms of the technique and quadrotors are different and hence, influence the chemical plume sensing process. Moths flap their wings to fly, generating low airflow disturbance. In contrast, quadrotors have four fast spinning propellers that continuously push air downwards to generate a resultant force that lifts the quadrotors upwards. This generates a strong airflow disturbance that affects the chemical plume sensing process. Therefore, researchers have proposed various types of enhanced or modified moth-inspired CPT techniques [4]–[6].

The performance of these proposed CPT techniques needs to be evaluated and compared. However, it is a challenging task as the results of these techniques are heavily influenced by environmental parameters, such as surrounding wind, humidity, and temperature. These environmental parameters are beyond researchers' control, especially in outdoor experiments, which extremely difficult to reproduce the same environmental parameters. In fact, both indoor and outdoor experiments also encounter repeatability problems. For instance, a researcher may find

it difficult to compare his proposed CPT technique with the CPT techniques of other researchers because reproducing the same environmental parameters is not feasible. Hence, to overcome this, a CPT simulator is the solution because the environmental parameters in a simulation can be easily reproduced.

Developing a CPT simulation model close to the real world also has its challenges. One of the main challenges is the high complexity of chemical plume disperser modelling. Marjovi and Marques [7] pointed out three types of chemical plume structure in various temporal scales: (1) Spatio-temporal variations with internal intermittency (STV-II) model (see Fig. 1(a) in caption); it is adapted from the real instantaneous plume structure with internal intermittency captured by planar laser-induced fluorescence technique of Crimaldi et al. [8]; (2) Spatio averaging and temporal variations (SATV) of the chemical plume simulation model (see Fig. 1(b) in caption); and (3) Spatio-temporal averaging (STA) of the chemical plume simulation model (see Fig. 1(c) in caption). STV-II model is still under development by researchers, some of the characteristics of this model such as plume meandering, internal intermittency, and vortices, have not been modelled in the previous studies before.

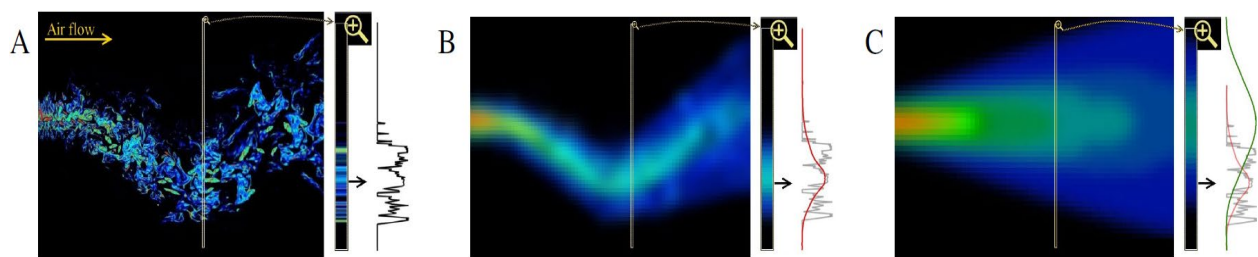


Fig. 1. Chemical plume structure in various temporal scales: (a) Spatio-temporal variations with internal intermittency (STV-II) model (adapted from [8]); (b) Spatio averaging and temporal variations (SATV) of the chemical plume simulation model ; and (c) Spatio-temporal averaging (STA) of the chemical plume simulation model [7].

Another main challenge is to model the impact of the flying mechanisms of quadrotors, for instance, to simulate the model of airflow disturbance generated by the propellers of quadrotors that affect the chemical sensing process. It is a critical factor that affects CPT results and also presents a research gap that needs to be addressed.

Simulating real-world environmental wind speed and vectors from fluid dynamics aspects and then integrating them into a CPT simulator is another challenge. In this case, we need a computational fluid dynamics (CFD) software to compute the wind vectors in a 3D space. The CFD software, moreover, has to be integrable into the CPT simulator.

In this study, we proposed a modification of the Gaussian-meandering plume propagation with internal intermittency modelling to simulate STV-II model (see Fig. 1). We also modelled the impact of the propellers of a quadrotor through an airflow analysis study. In addition, we used open-source CFD software, TYCHO [35], to generate an environment's wind vectors in a 3D space and then integrate them into our CPT simulator. These contributions can bring our 3D CPT simulator one step closer to real-world scenarios.

In the following sections of this paper, we discuss the significant related works and our proposed solutions in Section 2.0 and Section 3.0 respectively. Subsequently, the validation of the simulation and experimental results are discussed in Section 4.0, while the conclusion of our study is presented in Section 5.0.

## 2.0 RELATED WORKS

In the beginning, CPT simulation studies were mainly two-dimensional (2D) and graph-based representation [9]–[12]. An example is shown in Fig. 2. This simple model of a 2D CPT simulator can prove the concept or preliminary results of CPT algorithms such as chemotaxis, anemotaxis, and multi-robot solutions (e.g. particle swarm optimization (PSO), and gas distribution mapping [13]–[15]). Thus, it laid an important foundation for CPT studies. However, the simulator cannot provide accurate results because it does not include the real model of the robot; it only presents robot by a dot or mark, for example, a black circle dot (see Fig. 2). Therefore, the complexity model of a robot's moving mechanism (e.g. the airflow disturbance generated by the robot's movement) and the sensors' mounting position (e.g. the bilateral sensing system; left and right sensors' mounting position on the robot's structure) are neglected in this simple model.

Subsequently, Hayes et al. [16] made an important milestone when they developed their CPT simulator in a commercial robotics software, Webots, as shown in Fig. 3. They modelled a real-scale 3D robot model in their CPT simulation. They simulated a robot with the real-scale model, a Moorebot of 24 cm in diameter in a 6.7 x 6.7 m test field, and used the chemical plume propagation based on STA model in their CPT simulator. Some years later, Cabrita et al. [17] developed a CPT simulator in an open-source platform, Player/Stage simulation framework, as shown in Fig. 4. They simulated SATV model for the chemical plume propagation, however, they used a pre-defined meandering modelling, which attributes to the invariant of spatial characteristic. In addition, they used a commercial CFD software, ANSYS, to generate the wind vectors with obstacles in the test field; this was a significant contribution that imported CFD wind vectors into a CPT simulator. Besides that, they also used a well-known robot model, Roomba, in their CPT simulator. Khaliq [18] developed his CPT simulator in the most widely-used open-source platform, Robotics Operating System (ROS), as shown in Fig. 5. They also used an open-source CFD software, OpenFoam, to replace the commercial CFD software and simulated Spatio-temporal variations (STV) model of chemical plume propagation in their CPT simulator.

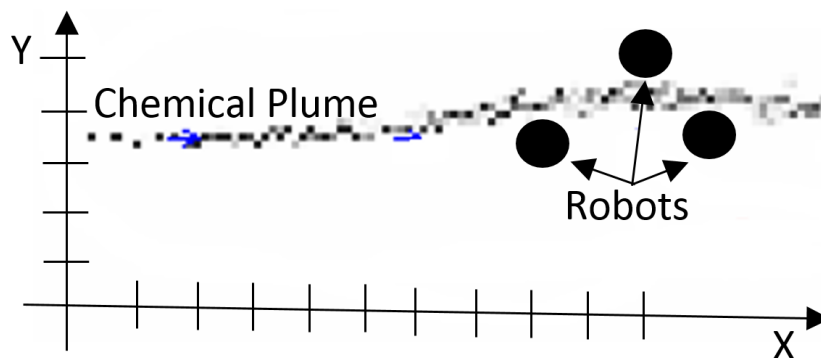


Fig. 2. Example of a 2D graph or numerical-based CPT simulation.

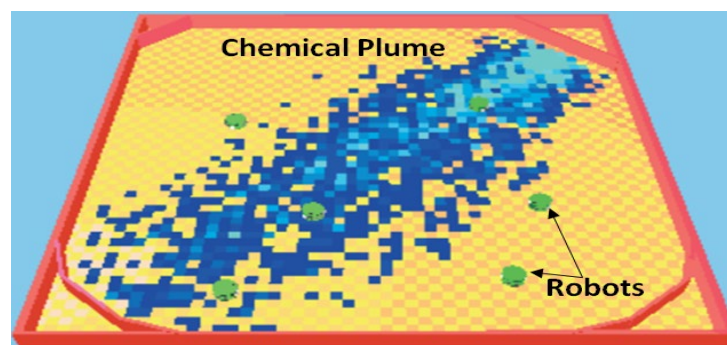


Fig. 3. CPT simulation in Webots by Hayes et al. [16].

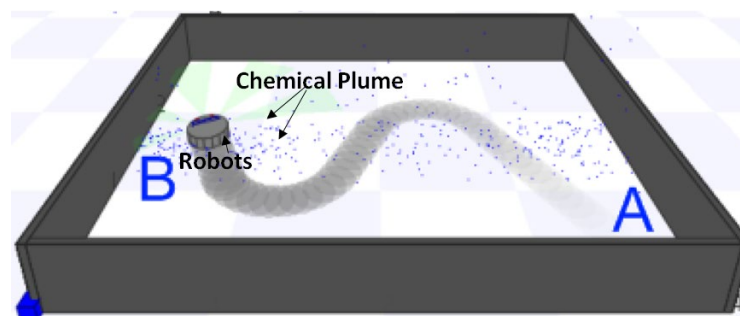


Fig. 4. CPT simulation in Player/Stage simulation framework by Cabrita et al. [17].

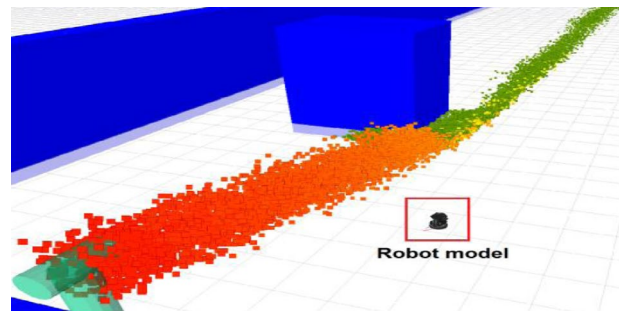


Fig. 5. CPT simulation in ROS platform by Khaliq et al. [18].

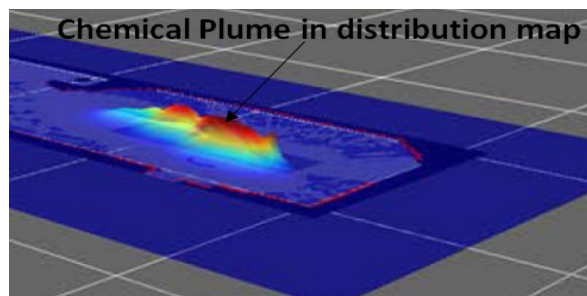


Fig. 6. CPT simulation in OpenMORA platform by Monroy et al. [19].

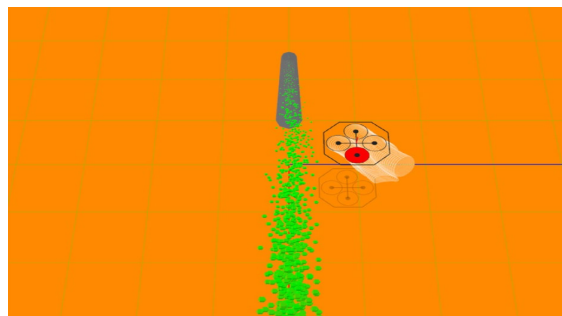


Fig. 7. CPT simulator with a quadrotor by Luo et al. [20].

As shown in Fig. 6, Monroy et al. [19] implemented a gas dispersion simulator in the OpenMORA platform with the enrichment of olfaction supporting functions such as gas distribution map, wind map, and navigation functions. STV model of chemical plume propagation was also adopted in their simulator. A subsequent study by Luo et al. [20] demonstrated a 3D CPT simulator with a quadrotor, as shown in Fig. 7. And the main contribution was on the aerodynamic olfactory effects of using numerical models. In another more recent study, Monroy et al. [21] developed a 3D gas dispersion simulator for mobile robot olfaction in realistic environments. Their simulator is able to support 3D computer-aided design (CAD) format files for simulating different environments and multiple sources of gas dispersions in a simulation.

To the best of our knowledge, the above mentioned six reported studies [16]–[21] are the only CPT simulators based on a 3D physics engine simulation framework with real-scale dimension of robot models found in the literature (other studies of 2D or 3D graph and numerical-based CPT simulators were not considered in the comparison because of their simplicity of modelling). Four of them [16]–[19] used the wheeled mobile robots, focusing mainly on 2D CPT tracing with the constant height of the wheeled robot. Monroy et al. [21] considered more realistic environments such as office building layout with multiple chemical plume sources in their simulator. Only Luo et al. [20] used a quadrotor but their main focus was the aerodynamic olfactory effects with numerical models, but not the meandering, internal intermittency, and vortices characteristics of chemical plume propagation model. Therefore, the consequential interaction between robot movement mechanism and chemical plumes is still underdeveloped because so far, only one reported study explored this [20].

All the CPT simulators in previous studies simulated only STV or SATV model of chemical plume propagation, where some of the characteristics of STV-II model such as plume meandering, internal intermittency, and vortices

have not been simulated in a 3D CPT simulator before and therefore, the main contribution of this study is to simulate STV-II model of chemical plume propagation.

### 3.0 PROPOSED SOLUTIONS

In this section, we discuss our rationale behind the selected physics engine-based robotics simulation platform used in our study and the modified Gaussian-meandering plume propagation with internal intermittency model in detail. We then present our analysis of the airflow disturbances generated by the quadrotor’s propellers and the propellers’ impact on the chemical plume sensing process in the simulation. Subsequently, we present the integration of our CPT simulator with an open-source CFD software, TYCHO, to simulate environment wind fields in a 3D space. Lastly, we present the gas sensors’ modelling used in our CPT simulator.

#### 3.1 Physics Engine- Based Robotics Simulation Framework for 3D CPT Simulation

Many physics engine-based robotics simulation frameworks, developed and maintained by open-source software communities, are available online. Each framework has its own strengths and weaknesses. To choose a suitable framework for our simulator, we compared them based on six criteria: type of license, type of physics engine, robotics middleware support, extensibility, varieties of robot models, and documentation support. Among all the choices, we chose the V-rep from Coppelia Robotics [22] because it fulfilled our requirements. V-rep is licensed under the GNU General Public License (GNU GPL or GPL), a widely used free software license which guarantees end users the freedom to run, study, share, and modify the software. It supports three types of physics engines – Open Dynamics Engine (ODE), Bullet, and Vortex – and also integrable with a popular robotics middleware like ROS and Sockets. In addition, it can be extended by C++ plugin and API and is able to provide a variety of robot models, such as ground mobile robots (UGV), robotic arms, humanoid robots, and most importantly, aerial robots (e.g. quadrotors). Last but not least, it also provides good documentation support.

#### 3.2 Chemical Plume Propagation Models

The chemical plume propagation model is the core of a CPT simulator in determining the propagation in a 3D space. A well-established model is the Gaussian gas dispersion model [23]–[25], which calculates the gas propagation’s concentration at the particulate x- and y-coordinates. Equation (1) and Fig. 8 show the mathematical model and illustration of the Gaussian gas dispersion model respectively. It is basically derived from two Gaussian concentration profiles: one for the y-axis and another for the z-axis. It is worth mentioning that, if a gas is lighter than atmospheric air, there will be a plume rise,  $\Delta h$ . Otherwise, it will be a plume drop. However, due to the high consumption of both computer processing power and elapsed time, it would be unsuitable to implement this model in a computational simulation.

$$C(x, y, z) = \frac{Q}{2\pi\sigma_y\sigma_z u} \exp\left(\frac{-y^2}{2\sigma_y^2}\right) \left( \exp\left(\frac{-(z-h)^2}{2\sigma_z^2}\right) + \exp\left(\frac{-(z+h)^2}{2\sigma_z^2}\right) \right) \quad (1)$$

Here,

- $C$  = Concentration at a given position
- $x$  = Downwind axis
- $y$  = Crosswind axis
- $z$  = Vertical direction
- $Q$  = Source emission rate
- $\sigma_y$  = Horizontal standard deviation of the emission distribution
- $\sigma_z$  = Vertical standard deviation of the emission distribution
- $u$  = Horizontal wind velocity along the plume centerline
- $h$  = High of the release

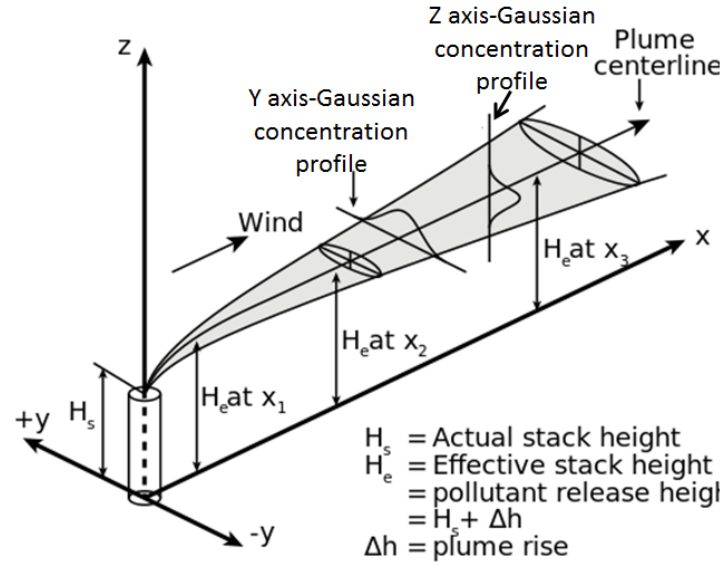


Fig. 8. Gaussian gas dispersion mathematical model [23].

Farrell et al. [10] proposed a significant alternative that has been widely adopted by most CPT simulators, the filament-based gas dispersion model, which is advantageous in both time- and memory-efficiency in computer processing consumption. In this model, a set of filaments ( $i = 0, 1, 2, \dots, n$ ) is used to simulate gas propagation. Each filament has its own attributes: position  $P_{i,t}$  and width  $R_{i,t}$ . For each time step  $t$ , the filaments' attributes are updated using equations (2) and (3). As expressed in equation (2), the position of the filaments is updated according to the wind flow  $V_{p,i,t}$  and an additional element, the Gaussian random factor  $\varepsilon_p$ . The Gaussian random factor, inherited from the Gaussian gas dispersion model, was added to model the turbulence and chaotic nature of gas propagation. The molecular diffusion is modelled in equation (3), where the width of the filament becomes wider with time while concentration decreases and the filament growth rate is denoted by a constant value,  $\gamma$ .

$$P_{i,t} = P_{i,t-1} + V_{p,i,t} \Delta t + \varepsilon_p \quad (2)$$

$$R_{i,t} = R_{i,t-1} + \frac{\gamma}{2R_{i,t-1}} \quad (3)$$

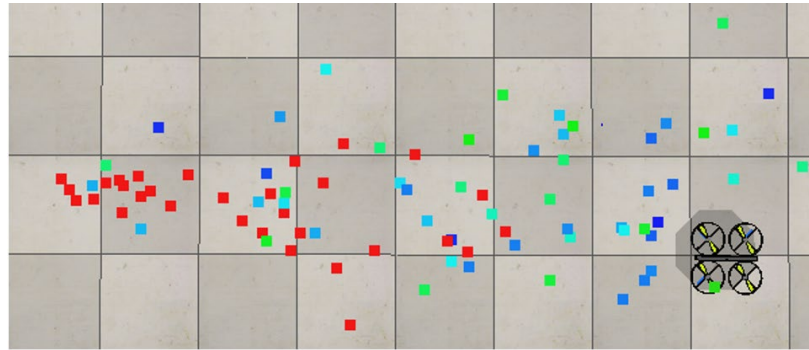
In this study, we modified the filament-based gas dispersion model from a 2D dispersion to a 3D dispersion. For the first implementation phase, we made two modifications. First, for the mathematical representation of 3D dispersion, each filament was presented in a four by one matrix array as shown in equation (4), where the first three rows represent the position of the filament in x-, y-, and z-coordinates and the last row is the width and odorant concentration of the filament. It is important to note that  $P_{z,i,t}$  was added with a plume rise,  $\Delta h$  (which assumes that chemical plume is lighter than atmospheric air, i.e. methane). If the chemical plume is heavier than atmospheric air, it will be plume drop instead, where  $\Delta h$  is a negative value. We then used a coloured heatmap with Hue colour value to represent odorant concentration. Hue colour value ranges from 0 to 255, indicating a colour gradient from red (highest concentration) to blue (lowest concentration). Hence,  $R_{i,t}$  was interpolated to the range of Hue $_{i,t}$  colour value, as stated in equation (5).

For this first implementation, we assumed constant wind vectors across the test field (dynamic wind vectors were considered in a later implementation phase). The illustration for this implementation is shown in Fig. 9(a) and it can be observed that the plume propagation is identical to STA model (see Fig. 1(c)).

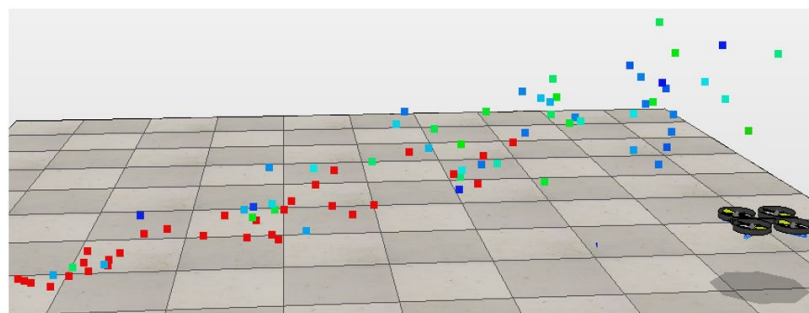
$$\begin{pmatrix} P_{x,i,t} \\ P_{y,i,t} \\ P_{z,i,t} \\ R_{i,t} \end{pmatrix} = \begin{pmatrix} P_{x,i,t-1} + V_{x,i,t} \Delta t + \varepsilon_x \\ P_{y,i,t-1} + V_{y,i,t} \Delta t + \varepsilon_y \\ P_{z,i,t-1} + V_{z,i,t} \Delta t + \Delta h + \varepsilon_z \\ R_{i,t-1} + \frac{\gamma}{2R_{i,t-1}} \end{pmatrix} \quad (4)$$

$$\forall i \in \{1, \dots, n\}$$

$$Hue_{i,t} = \frac{255 (R_{i,t-1} - R_{min})}{(R_{max} - R_{min})} \quad (5)$$



(a)



(b)

Fig. 9. The illustration of STA model. (a) Top view and (b) Isometric view.

We proceeded to the second implementation phase, which was to model the features of SATV model (see Fig. 1. (b)). SATV model has an instantaneous plume boundary feature, where the plume propagation meanders gently through the atmosphere, as shown in Fig. 10. This meandering feature (curving and winding in shape, like a snake when it moves) is the key element of SATV model. To embrace this feature in our model, we adopted the fluctuating plume dispersion model (FPM), proposed by Gifford, F. [26]. This model is scientifically proven and widely recognized by researchers in their studies [27]–[31]. In this model, the Gaussian plume boundary can be thought of as a series of plume segment, as shown in Fig. 11 (a) & (b). The position of a filament calculated by the FPM is a result of two Gaussian distributions. As refer to Fig 11 (c):  $\sigma_c$ , determines the location of plume segment centreline;  $\sigma_p$ , defines the instantaneous boundary within the plume segment.

Based on this premise, we needed to modify equation (4) to compute the instantaneous plume meandering features, by adding a parameter, plume segment Pseg, to determine the total number of plume segmentations in a plume propagation. Each plume segment has two elements:  $\sigma_c$  and  $\sigma_p$ , this means, these can be expressed as  $\{(\sigma_{yc1}, \sigma_{zc1}), (\sigma_{yc2}, \sigma_{zc2}), (\sigma_{yc3}, \sigma_{zc3}), \dots (\sigma_{ycPseg}, \sigma_{zcPseg})\}$  and  $\{(\sigma_{yp1}, \sigma_{zp1}), (\sigma_{yp2}, \sigma_{zp2}), (\sigma_{yp3}, \sigma_{zp3}), \dots (\sigma_{ypPseg}, \sigma_{zpPseg})\}$ , were assigned by the concentration probability density function (PDF) that determined by meander ratio (Yee et al. [28] correlated between meander ratio and its concentration PDF). These defined the center line and the instantaneous boundary of plume segments. Subsequently, equations (6) and (7) will be computed filaments ( $i = 0, 1, 2, \dots n$ ), for each iteration. Equation (6) determines the meandering features, according to the sequence of plume segment of the filament's travelling distance in the simulation. After that, meandering features to be substituted into equation (7), to update all the filaments' position with the influence of meandering feature. For the next iteration, a new set of meandering features is generated again, hence, the dynamical meandering feature was modelled.

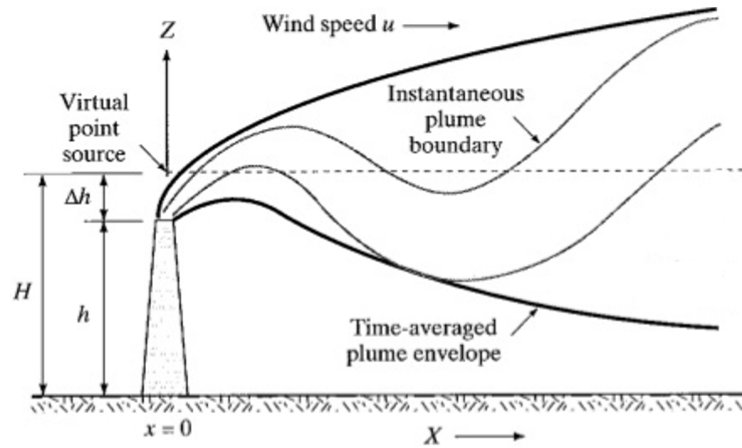


Fig. 10. Gas dispersion model with instantaneous plume boundary [23]

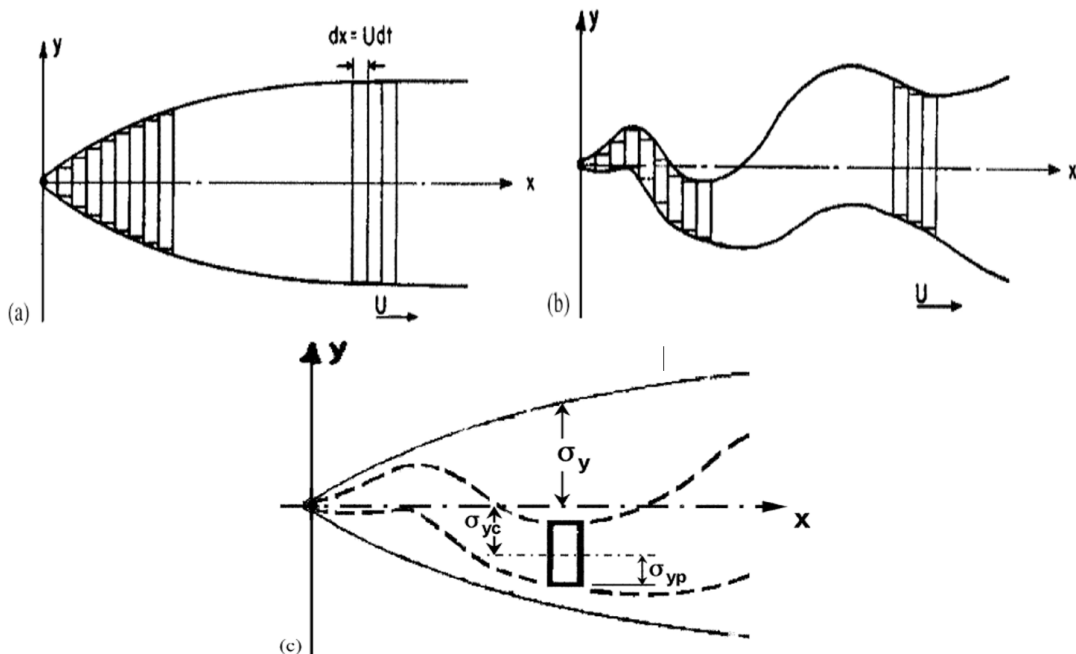


Fig. 11. a) Plume segments in Gaussian plume model; (b) Plume segments in fluctuating plume model; (c) standard deviations of fluctuating plume model.

$$\begin{bmatrix} \sigma_{yc} \\ \sigma_{yp} \end{bmatrix} = \begin{bmatrix} \sigma_{ycj} \\ \sigma_{ypj} \end{bmatrix}$$

$$\begin{bmatrix} \sigma_{zc} \\ \sigma_{zp} \end{bmatrix} = \begin{bmatrix} \sigma_{zcj} \\ \sigma_{zpj} \end{bmatrix} \quad (6)$$

where,  $j = \left\| \frac{\text{Current filament travel distance}}{\text{Maximum plume distance in simulation}} \times \text{Pseg} \right\|$

$$\begin{pmatrix} P_{x_{i,t}} \\ P_{y_{i,t}} \\ P_{z_{i,t}} \\ R_{i,t} \end{pmatrix} = \begin{pmatrix} P_{x_{i,t-1}} + V_{x_{i,t}} \Delta t + \varepsilon_x \\ P_{y_{i,t-1}} + V_{y_{i,t}} \Delta t + \sigma_{yc} + \sigma_{yp} \\ P_{z_{i,t-1}} + V_{z_{i,t}} \Delta t + \Delta h + \sigma_{zc} + \sigma_{zp} \\ R_{i,t-1} + \frac{\gamma}{2R_{i,t-1}} \end{pmatrix} \quad (7)$$

$\forall i \in \{1, \dots, n\}$



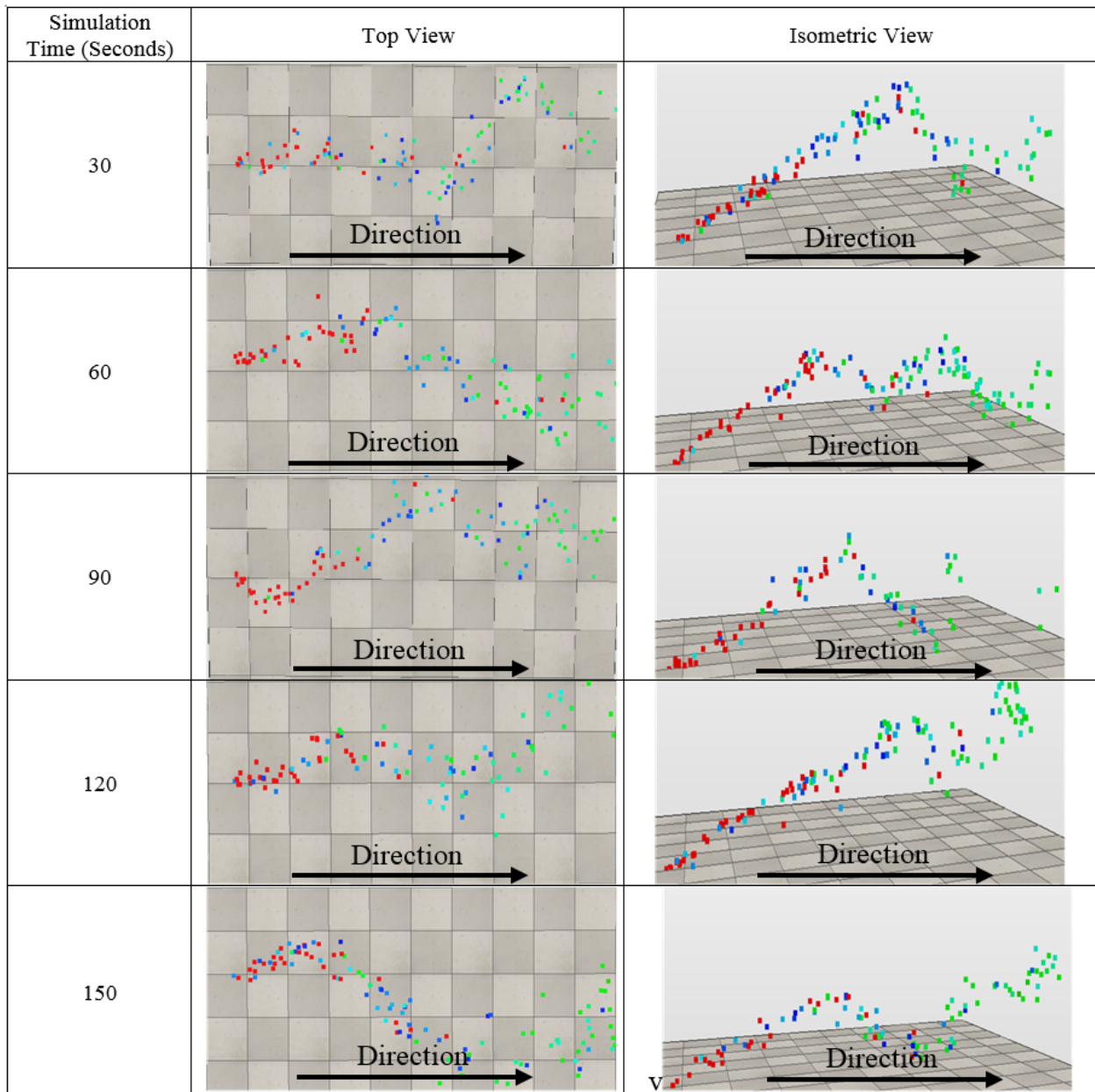


Fig. 12. The illustration of SATV model at different simulation times.

Fig. 12 illustrates the second implementation, where the gas propagation meanders gently through the atmosphere at different simulation times. The meandering feature of SATV model is clearly presented in the top view of Fig. 12, from simulation time 30 seconds to 150 seconds, proving the time-variant of the model. At this point, we have surpassed the previously reported study, the pre-defined meandering model [17], and introduced a new dynamical meandering of SATV model.

STV-II model, a real instantaneous plume structure with internal intermittency, was captured by Crimaldi et al. [8] with the use of planar laser-induced fluorescence technique. Their results demonstrated the following characteristics of STV-II model: patchy, intermittent, random vortices, and time-variant. The principal cause of these characteristics is the parcels of chemical substances that contain high concentrations of odorants released from a source and spread into filaments by shearing in the turbulent air. These filaments stir around in eddies and intermingle with the surrounding air and hence, chemical plumes become scattered in intermittent patches [32]. The level of intermittent patches was determined by Reynolds number ( $Re$ ), defined as the ratio of inertial forces to viscous forces which consequently quantifies the relative importance of these two types of forces for the given flow conditions. In short, a higher value of  $Re$  causes a stronger turbulent air and more severe intermittent patches of plume structure.

For the third implementation phase, we expressed STV-II model's characteristics into three attributes: intermittency, patch size, and random vortex. These attributes are the subset of each filament ( $i = 0, 1, 2, \dots, n$ ). It means that after computing the meandering point and filaments' position (using equations (6) and (7) in the second implementation), we computed these attributes by using equations (8) and (9) in every iteration. For equation (8), we derived the standard deviation of the attributes, which are proportionate to  $Re$ , with each having constant parameters  $a$  and  $b$ . The initial conditions are assigned as follows:  $ps_{i,t=0} \leftarrow \text{random}(a,b)$ , and  $rV_{i,t=0} \leftarrow \{N(\alpha, \sigma_{rv}), N(\gamma, \sigma_{rv}), N(\gamma, \sigma_{rv}), N(\gamma, \sigma_{rv})\}$ . Equation (9) shows each attribute varied from time to time and is influenced by Gaussian distribution  $\epsilon_{ps}$ , and  $\epsilon_{rV}$  respectively; these Gaussian distributions' standard derivations were proportionated to  $Re$ . One of these two attributes has its own subset elements, which is random vortex. It has four elements such as radius  $r_{i,t}$  and angle degrees  $\Theta_{xi,t}$ ,  $\Theta_{yi,t}$ , and  $\Theta_{zi,t}$ . These elements were used to compute the random vertices' shape by using equation (10).

$$\begin{aligned}\sigma_{ps} &= a(Re) \\ \sigma_{rV} &= b(Re)\end{aligned}\tag{8}$$

$$\begin{pmatrix} ps_{i,t} \\ rV_{i,t} \end{pmatrix} = \begin{pmatrix} ps_{i,t-1} + \epsilon_{ps} \\ rV_{i,t-1} + \epsilon_{rV} \end{pmatrix}$$

$\forall i \in \{1, \dots, n\}$

$ps = \text{patch size}$   
 $rV = \text{random vortex}$   
 $\epsilon_{ps} = N(\mu_{ps}, \sigma_{ps})$   
 $\epsilon_{rV} = N(\mu_{rV}, \sigma_{rV})$

$$rV_{i,t,k} = \begin{pmatrix} r_{i,t,k} \\ \theta_{x,i,t,k} \\ \theta_{y,i,t,k} \\ \theta_{z,i,t,k} \end{pmatrix} = \begin{pmatrix} r_{i,t-1} + |N(\alpha, \sigma_{rv})| \\ N(\gamma, \sigma_{rv}) \\ N(\gamma, \sigma_{rv}) \\ N(\gamma, \sigma_{rv}) \end{pmatrix}\tag{9}$$

$$\begin{pmatrix} P_{xk} \\ P_{yk} \\ P_{zk} \end{pmatrix} = \begin{pmatrix} P_{xi,t} + r_{i,t,k} \cos(\theta_{x,i,t,k}) \\ P_{yi,t} + r_{i,t,k} \cos(\theta_{y,i,t,k}) \\ P_{zi,t} + r_{i,t,k} \cos(\theta_{z,i,t,k}) \end{pmatrix}\tag{10}$$

$\forall k \in \{1, \dots, ps\}$

Fig. 13. illustrates the third implementation phase and the characteristics of STV-II model. To pinpoint these characteristics, we highlighted two patches of particles, patch N and K, at different timings. The propagation of patch N and K can be observed as gradually expanding their vortices' shape by random factors from simulation time 11 seconds to 55 seconds.

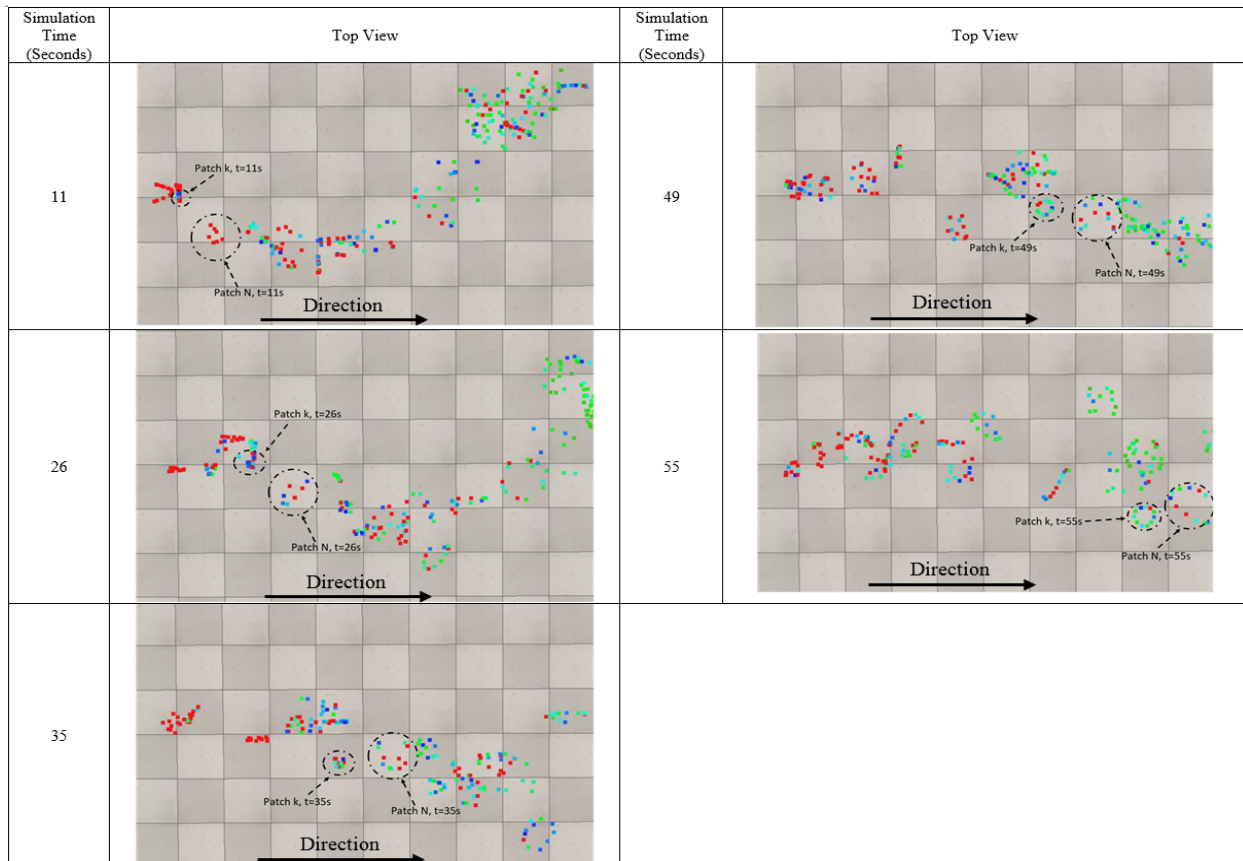


Fig. 13. The illustration of STV-II model's characteristics: patchy, intermittent, random vortices, and time-variant at different timings.

### 3.2 The Impact of The Model of Flying Mechanisms

Quadrotors use aerodynes approach to fly, whereby upwards lift is gained through multi-rotors and hence, strong airflow disturbances are generated during flights. This has a big impact on the chemical plume sensing process; for instance, blowing away chemical plumes before sensors can detect them.

To understand how generated airflow disturbances affect the sensing process, we conducted an airflow analysis by using a 3D Model CFD software, SolidWorks' flow simulation function [6]. From the simulation result as shown in Fig. 14, the airflow pattern is represented by dash lines and the airflow direction is represented by arrows. We discovered that there are four main air streams of air intake into four different propellers. Each airstream has three regions such as air intake, airflow eddies, and air exhausts. First, the air intake region shows how surrounding air is sucked into the propellers. Second, the airflow eddies region circulates airflow back into the propellers- it is only formed during the altitude of the quadrotor is changing[33]. Lastly, the air exhaust region is where the air leaves the system.

For the fourth implementation phase, we incorporated the airflow patterns of quadrotors in our CPT simulation. The airflow vectors of the quadrotor's airflow disturbances were modelled in the CPT simulation and applied within the approximated boundary of the quadrotors' airflow patterns. Fig. 15 shows the comparison between the without and with propeller's impact model (one of the propellers' impacts on the plume filaments is simulated in Fig. 15). As seen in the left column of Fig. 15 (without propeller's impact model), during the simulation time between 1 and 3 seconds, plume filaments pass above the quadrotors and hence, the gas sensor detects nothing. In contrast, the right column of Fig. 15 (with propeller's impact model) shows some of the chemical plume filaments being sucked into the propeller's airflow zone. At this moment, the gas sensor detects the filaments. Taking a closer look at simulation time from 0.1 to 0.6 seconds, where the altitude of the quadrotor is increasing (see Fig. 16), we can see the effect of airflow eddies. During the simulation time from 0.1 to 0.2 seconds, the highlighted plume filaments are sucked into the propeller. Between the simulation times of 0.3 and 0.5 seconds, some of the highlighted plume filaments are affected by the airflow eddies, circulating back to the propeller again, while the rest of the plume filaments leave the

propeller system. Finally, those circulated plume filaments pass through the propeller for the second time and then leave the propeller system at simulation time 0.6 seconds.

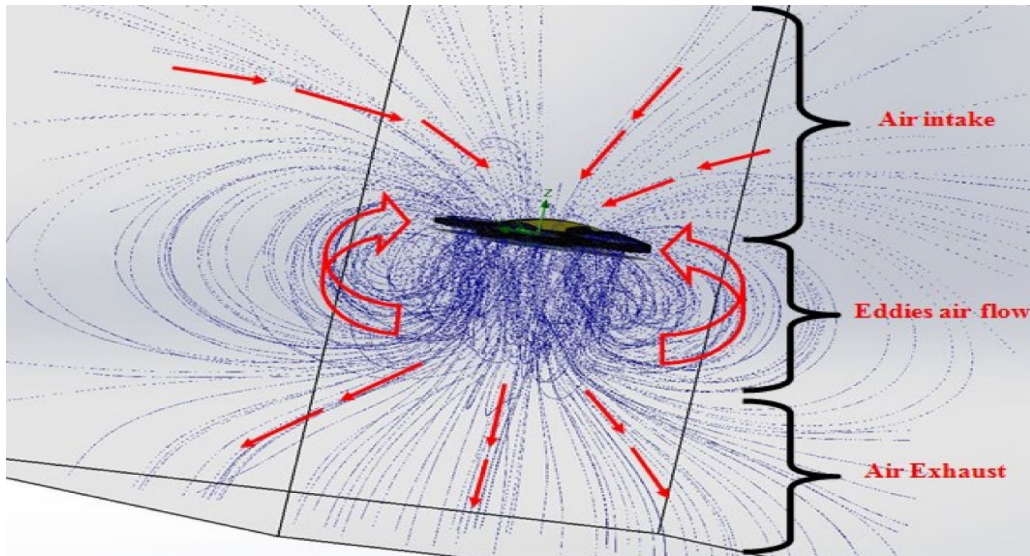


Fig. 14. Simulation result of airflow analysis of a quadrotor.

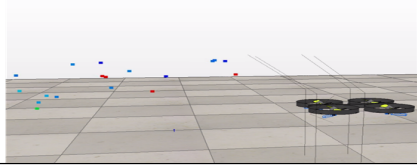
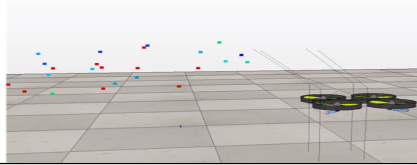
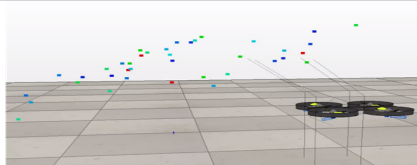
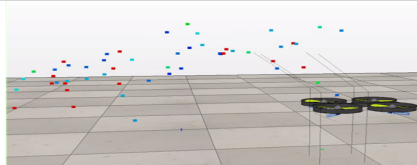
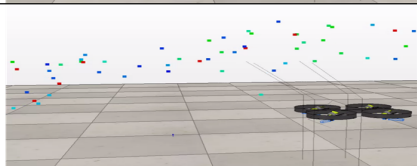
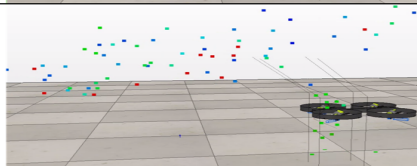
Simulation Time (Seconds)	Without propellers' impact	With propellers' impact
1		
2		
3		

Fig. 15. Comparison between the without and with propeller's impact model.

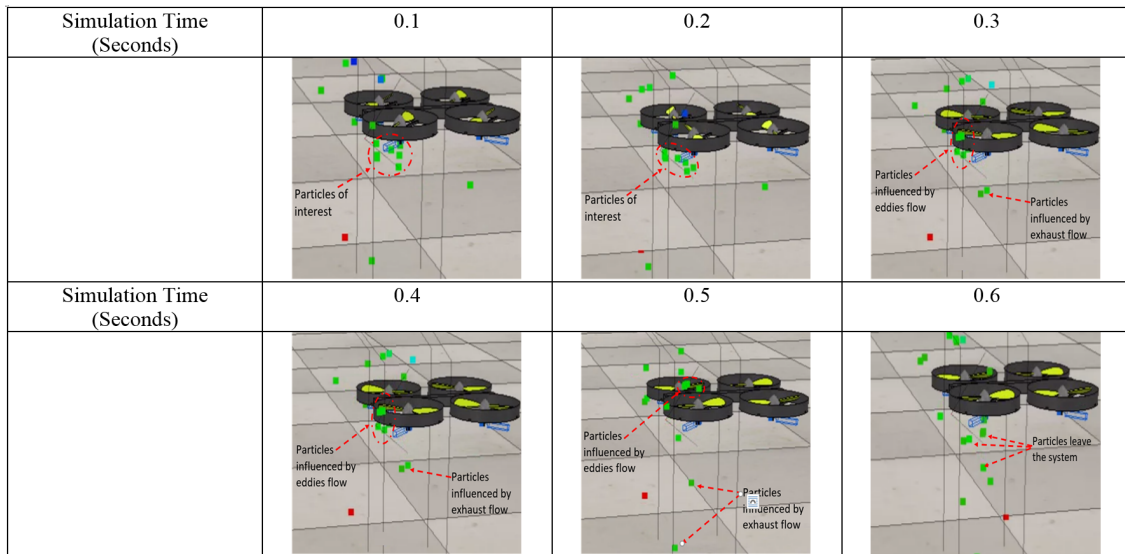


Fig. 16. Propeller's impact model for airflow eddies.

### 3.3 Integration with Computational Fluid Dynamics (CFD)

For the fifth implementation phase, we needed to simulate the realistic effect of environment windbreaks on the chemical plume propagation. A CFD software had to be used to compute every single airflow vector in the 3D space of interest. It is a numerical approach, which iteratively solves the conservation equations for mass, momentum, and energy in a finite volume of fluid dynamics problems. Therefore, the accurate airflow vectors computed by the CFD software can be substituted into the wind parameters ( $V_{x,i,t}$ ,  $V_{y,i,t}$ , and  $V_{z,i,t}$ ) in equation (7) to simulate the realistic chemical plume propagation, especially if there are obstacle blocks in the space of interest. For instance, a tree, a building block, or even a small hill, increases the complexity of the airflow vectors and plume propagation. With the use of the CFD software, the complicated airflow vectors can be calculated [34].

We chose open-source CFD software, TYCHO [35], which is a 3D compressible hydrodynamics written in C and parallelized with OpenMP, and a Lagrangian remapped version of Piecewise Parabolic method. One of the advantages of TYCHO is that it offers a simulation of gas-obstacle interaction with obstacles in wind-streams and advection of marker fields. In addition, momenta and their direction on obstacle-surfaces, thermal diffusion, and viscosity can be studied in the simulation [36].

For this integration, TYCHO generated a static windbreaks scenario of airflow vectors with a resolution of 375,000 data points in a  $125 \text{ m}^3$  of a 3D space (see Fig. 17). All these airflow vectors were exported to a data file and then imported into our CPT simulation. Thus, the wind parameters ( $V_{x,i,t}$ ,  $V_{y,i,t}$ , and  $V_{z,i,t}$ ) in equation (7) were substituted by the imported airflow vectors. Finally, the plume propagation that reflects the windbreaks results of TYCHO with one obstacle block and two obstacle blocks are shown in Fig. 18 and Fig. 19 respectively.

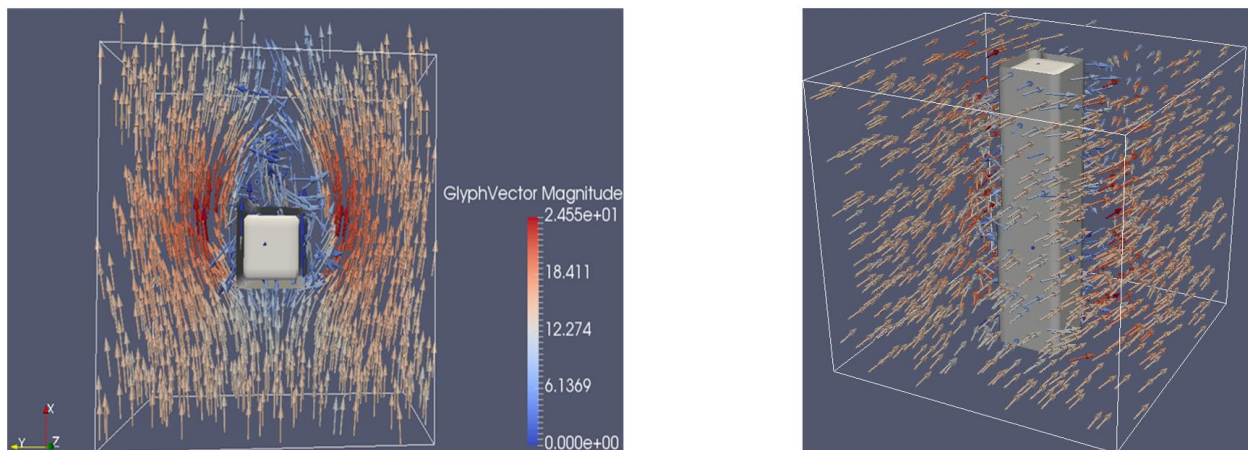
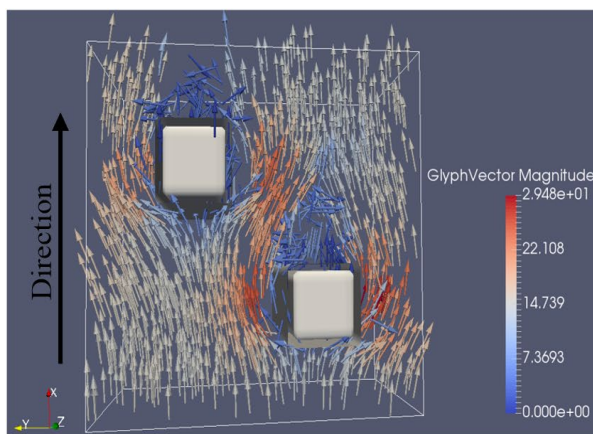


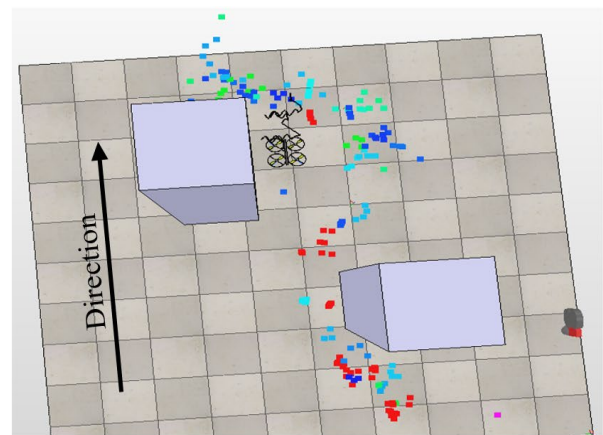
Fig. 17. 3D airflow vectors with single obstacle block generated by TYCHO.



Fig. 18. 3D plume propagation reflects the windbreaks with single obstacle block.



(a)



(b)

Fig. 19. 3D plume propagation reflects the windbreaks with two obstacle blocks.

### 3.4 MOX Sensors Modelling

For the last implementation phase, we modelled the gas sensors used in our CPT simulator. We used the semiconductor metal-oxide (MOX) gas sensors, commonly used in industries, because of their high sensitivity and fast response time in gas sensing. The sensor has a fast response in detecting gas but requires a very long recovery time after the exposure of the target gas [37], [38]. It takes around 15 to 70 seconds for the sensor to return to the baseline level after the target gas is removed [39].

We referred to the sensor models proposed by Khaliq et al. [18], such as filament-based concentration calculation and sensor response generation, to model the sensors in our CPT simulator. It is worth mentioning that we set the rise time parameter,  $\tau_r$ , at 15 seconds and decay time parameter,  $\tau_d$ , at 70 seconds for the rise and decay time model as stated in equations (11) [18] and (12) [18]. This is to model the sensor's response closer to the real-world MOX sensor, especially since the long recovery time of MOX sensors has a significant impact on the performance of CPT algorithms. If we neglected this in our simulator, the performance of the CPT algorithms cannot be fairly evaluated. The overall illustration of our CPT simulator is shown in Fig. 20, where the graphs of gas sensors' reading are shown on top of the simulator.

$$f_t = \alpha y_t + (1 - \alpha)f_{t-1} \tag{11}$$

Here,  
 $f_t$  = Filtered output  
 $\alpha$  = Smoothing factor  
 $y_t$  = Input sensor response

$$\alpha = \frac{dt}{\tau + dt} \tag{12}$$

Here,  
 $dt$  = Time interval  
 $\tau$  = Time constant

The overall concept of the CPT simulator is shown in Fig. 21 [40], the overall idea of integration between the gas dispersion simulator and MRO simulator is adopted and modified from Ali Khaliq et al [41]. The CPT simulator allows users to define their inputs: the robot model, wind flow vectors from CFD software, and environment models such as obstacles, walls, and layout. As the simulator started, gas dispersion simulator will generate the chemical/gas filaments and its propagation. Quadrotor propellers modelling will take effects to those chemical/gas filaments that near to it, for example, sucks in or blow away the filaments. Subsequently, sensors modelling will be updated according to the contact between sensors and filaments. Lastly, the sensors' responses will be inputted to mobile robot olfaction (MRO) algorithm, for controlling the tracing actions. Users can program different MRO algorithms to evaluate the performance of the algorithms.

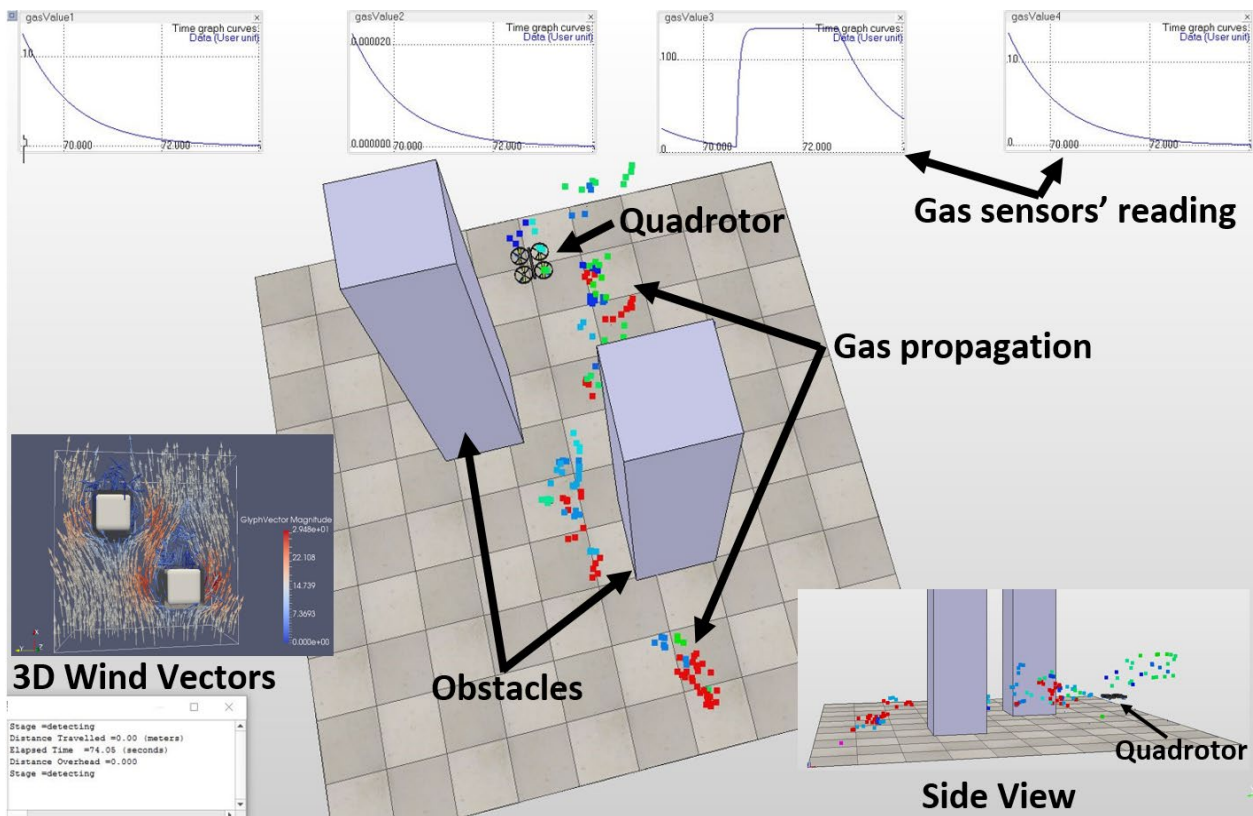


Fig. 20. The overall illustration of the CPT simulator

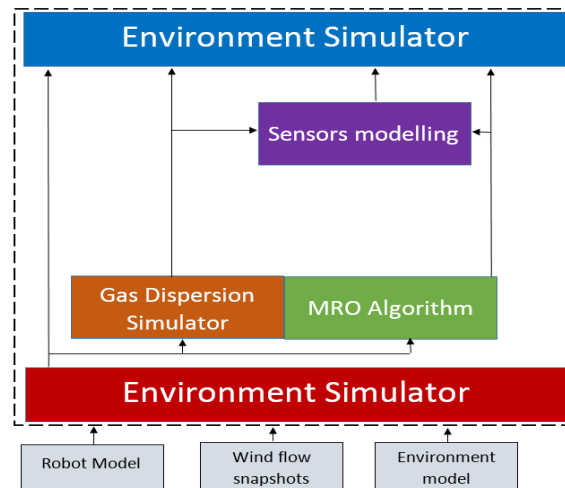


Fig. 21. The block diagram of the CPT simulator [40]

### 3.5 Chemical Plume Tracing Algorithm

In this paper, Moths' olfactory tracking strategy (also known as Zigzag algorithm), is used to complete the CPT [42]. When the chemical plume is detected, moth will track closely to the chemical plume along the wind direction with stereo sniffing: left- or right- forward tracing. This action is called the upwind surge. However, the pattern of chemical plume is nonlinearity, therefore the moth might lose track of the chemical plume during the surging behavior. For this reason, whenever the moth failed to track the chemical plume, it will perform zigzag movement orthogonal to the wind direction and slowly increases its zigzag wavelength after each iteration. This action is called casting, as shown in Fig. 22. Once, the moth is back on the track, it performs upwind surge again. The process of switching upwind surge and zigzag casting would continue until the chemical source is located.

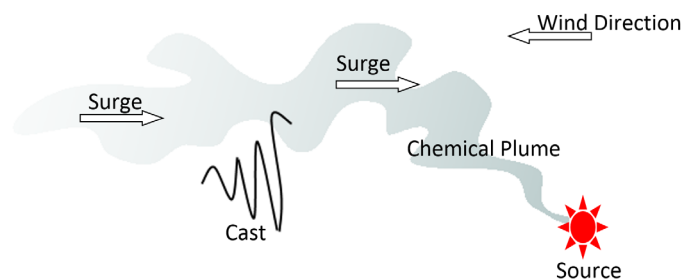


Fig. 22. Moths' olfactory tracking strategy

## 4.0 EXPERIMENTAL RESULTS AND DISCUSSIONS

To validate the performance of our CPT simulator, we conducted two types of experiment: (a) the comparison of the responses of the sensors between simulation and real-world environment; and (b) the comparison of the CPT trajectory paths between simulation models of STA, SATV, and STV-II with real-world. The first type of experiment is to prove that the responses of the sensors of the simulation are in an agreement with real-world. The second type of experiment is to validate the CPT trajectory paths of these three simulation models with real-experiment, to verify which model is closer to reality.

### 4.1 The Comparison of the Sensors Responses between the Simulation and Real-World

We conducted an experiment with three different sensing scenarios. The chemical plume generator was located at different orientations,  $45^\circ$ ,  $0^\circ$ , and  $-45^\circ$  (see Fig. 23) to study the sensors' responses in each scenario. For the real-world experiment setup, we built a chemical plume generator, as shown in Fig. 24(a), and developed a quadrotor-based CPT robot equipped with four gas sensors at different configurations, such as back-left, front-left, front-right, and back-right sensors (see Fig 24(b)). Subsequently, we compared the sensing scenarios in both the experiment and simulation.



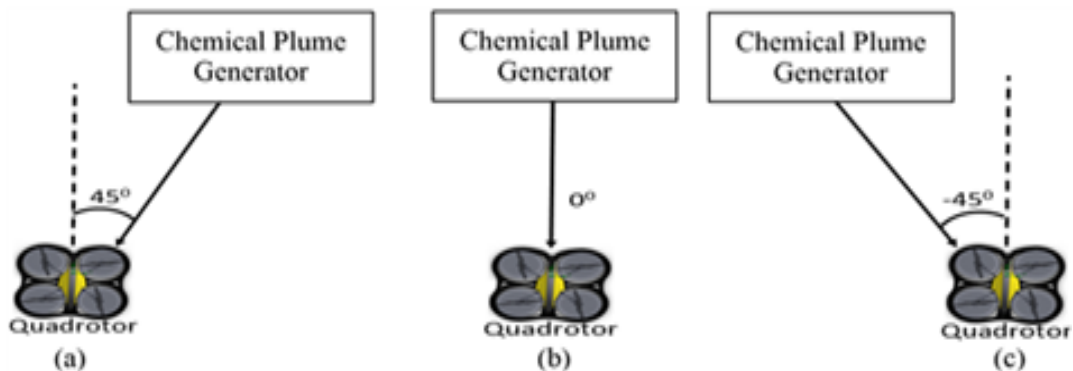


Fig. 23. (a) Experiment scenario A: 45° degree angle (right-hand side) to quadrotor; (b) Experiment scenario B: 0° degree angle (center) to quadrotor; and (c) Experiment scenario C: -45° degree angle (left-hand side) to quadrotor.



Fig. 24. The experiment setup. (a) Chemical plume generator and (b) Quadrotor armed with four gas sensors.

Based on Fig. 25, the simulation results of the sensing ratio (in between the four gas sensors) are approximate to the experimental results, under a condition that the simulation sensing models have been tuned and calibrated in prior. In particular, simulation scenario (a) shows that the front-right sensor detected the highest chemical plume concentration or parts per million (PPM), the front-left sensor detected the second highest PPM, the back-right sensor detected low PPM, and the back-left sensor detected nothing. Likewise, in experiment scenario (a), the sensing ratio was approximate to the one in the simulation. The only difference was that the back-left sensor in the experiment detected a very low PPM because real-world sensors are oversensitive and have a linearity error at a particular range of sensing. The sensing ratio in the simulation and experiment was similar for both scenarios (b) and (c), with the exception of the oversensitivity of the real-world sensor.

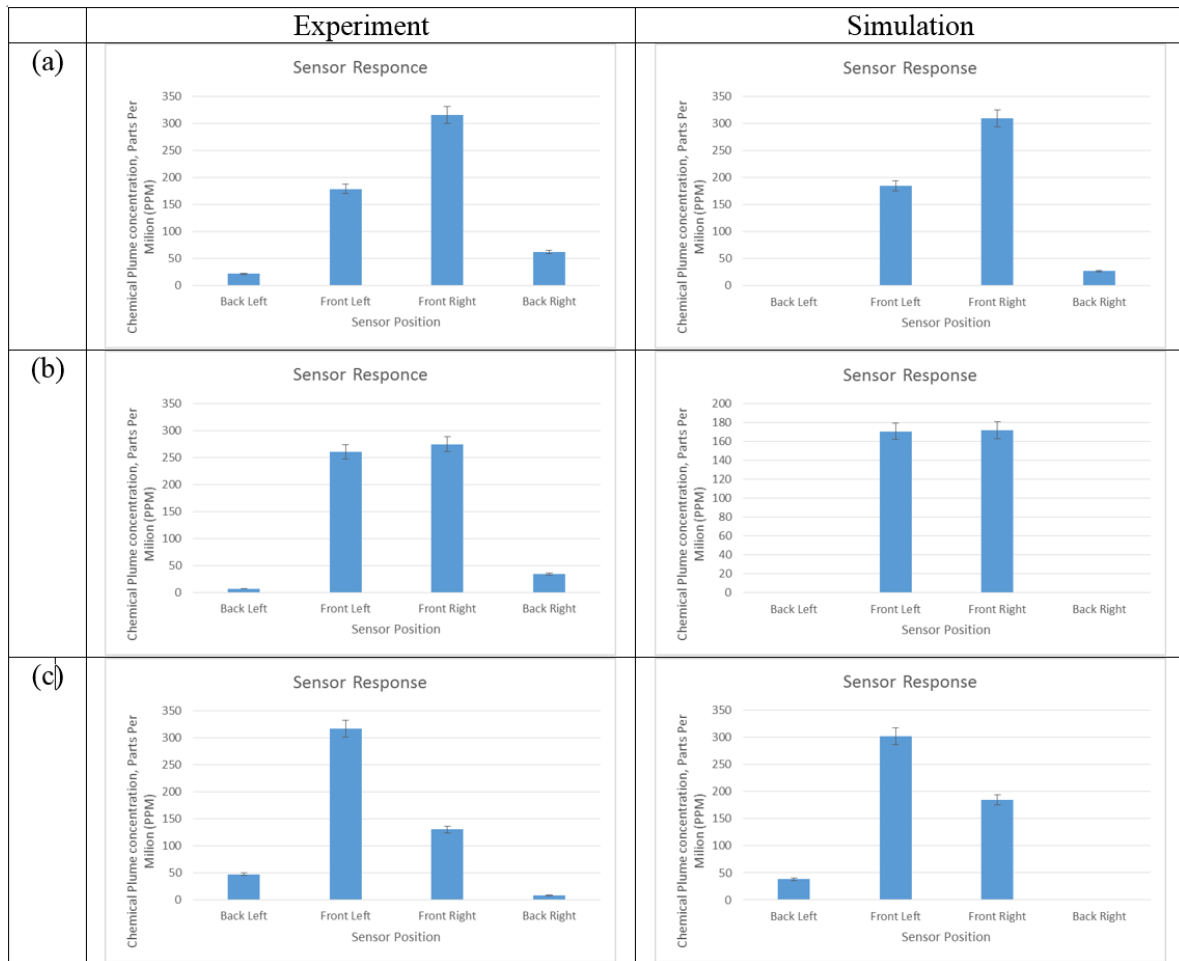


Fig. 25. The comparison of results between experiment and simulation

#### 4.2 The Comparison of the Chemical Plume Tracing Trajectory Paths Between Simulation Models Of STA, SATV, STV-II And Real-World

The performance of CPT trajectory path towards chemical plume source is heavily influenced by the characteristics of chemical plume propagation such as meandering, internal intermittency, and vortices. These characteristics hinder the CPT performance, in this case, the distance overhead and elapsed time will be increased and causes CPT trajectory path will be more curving and twisting. Distance overhead is defined as the total travelled distance divided by the distance of the shortest path to the source. A smaller distance overhead value indicates better performance. Similarly, a shorter elapsed time indicates better performance. The comparison of the CPT trajectory path between real-world and simulation models can indicate which simulation model is closer to reality.

Fig. 26, Fig. 27, and Fig. 28 show the trajectory paths of simulation models of STA, SATV, and STV-II. The results show that STA model has lowest distance overhead and elapsed time, 1.823 and 463.9 seconds, respectively (see Fig. 31). To justify these results, we can observe from Fig. 26, the trajectory paths of STA model has the smallest fluctuation, where the standard deviation  $\sigma$  of 0.123. The main reason for getting a smooth trajectory path because of the idealistic of the modelling, which is too even-distributed in its propagation. However, it is unlikely in a realistic scenario.

SATV model has distance overhead of 2.355 and elapsed time of 678.6 seconds. The CPT performance of SATV model is poorer than STA model because of the meandering feature of SATV model, which has increased the fluctuation of trajectory paths with standard deviation  $\sigma$  of 0.2508 (see Fig. 27), and causes difficulties in the tracing process.

The last simulation model of STV-II, the fluctuation of trajectory paths has increased the standard deviation  $\sigma$  to 0.3433 (see Fig. 28) because of its internal intermittency and vortices features. These two features cause higher

chances of losing track of the chemical plumes, thus causes bigger fluctuation of trajectory path; both distance overhead and elapsed time have increased to 3.42 and 886.3 seconds, respectively.

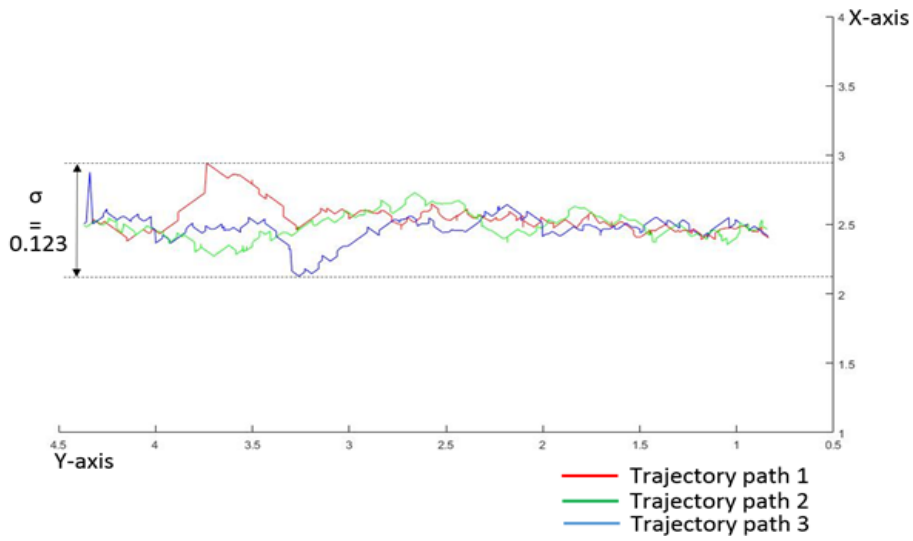


Fig. 26. The trajectory paths of STA simulation model

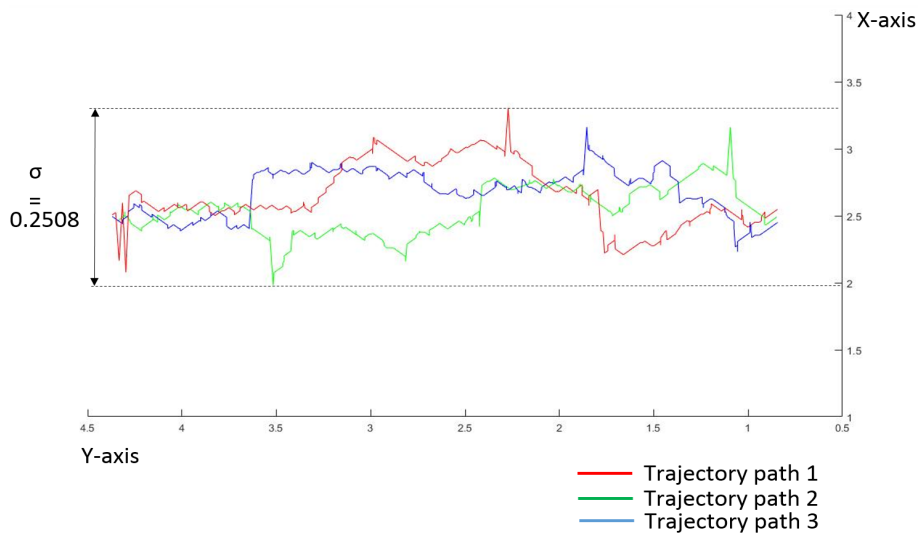


Fig. 27. The trajectory paths of SATV simulation model

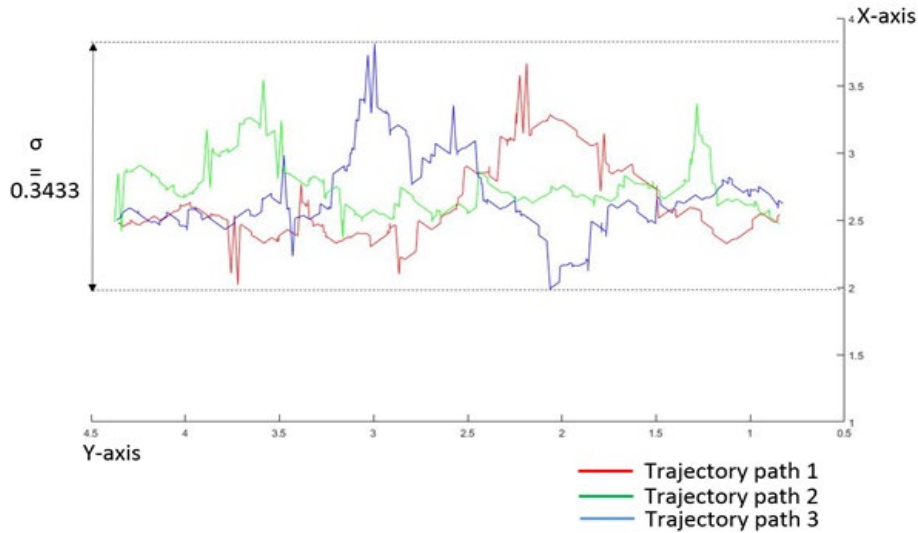


Fig. 28. The trajectory paths of STV-II simulation model

To validate the simulation models, we conducted the real-world experiment with our quadrotor-based CPT robot, as shown in Fig 29, the quadrotor is equipped with four gas sensors: back-left, front-left, front-right, and back-right sensors. We put an image marker on top of quadrotor, for the purpose of the indoor image processing based positioning system. As compared with simulation results, as shown in Fig 30 and 31, STV-II model has closer results to real-world, which is under the controlled environment (the indoor experiment as shown in Fig 29). This can be observed from the standard deviation  $\sigma$  of the trajectory paths (see Fig. 28 and Fig. 30), has an error percentage of 12.95%, and the error percentage for distance overhead and elapsed time are 16.17% and 10.97% (see Fig. 31).

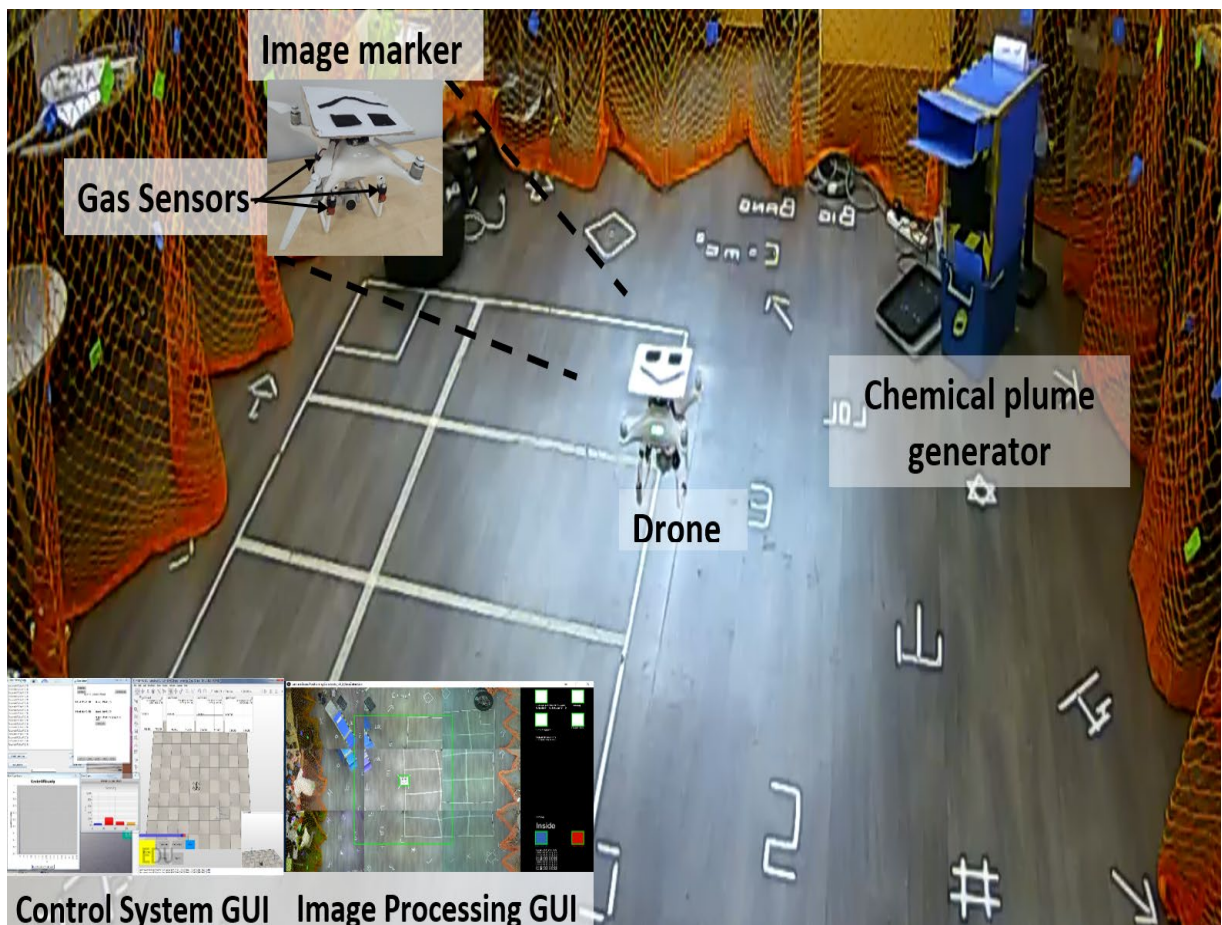


Fig. 29. The real-experiment setup

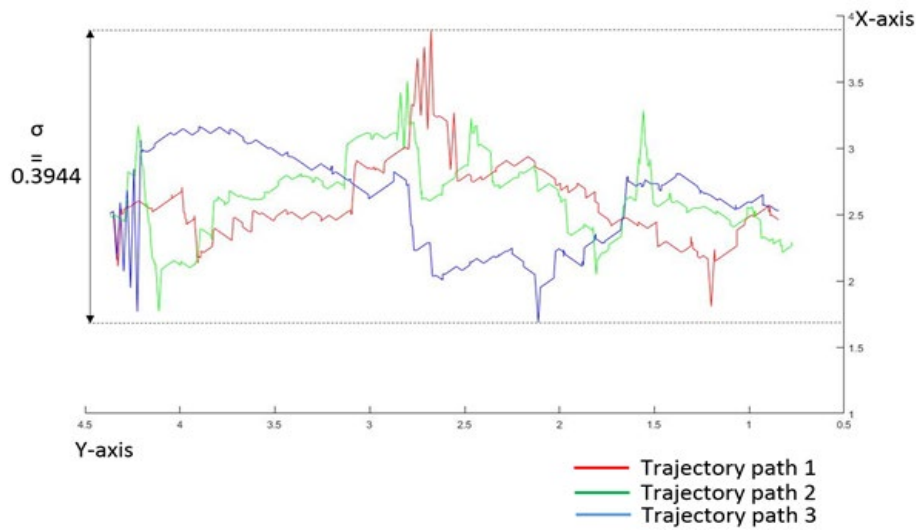


Fig. 30. The trajectory paths of real-experiment

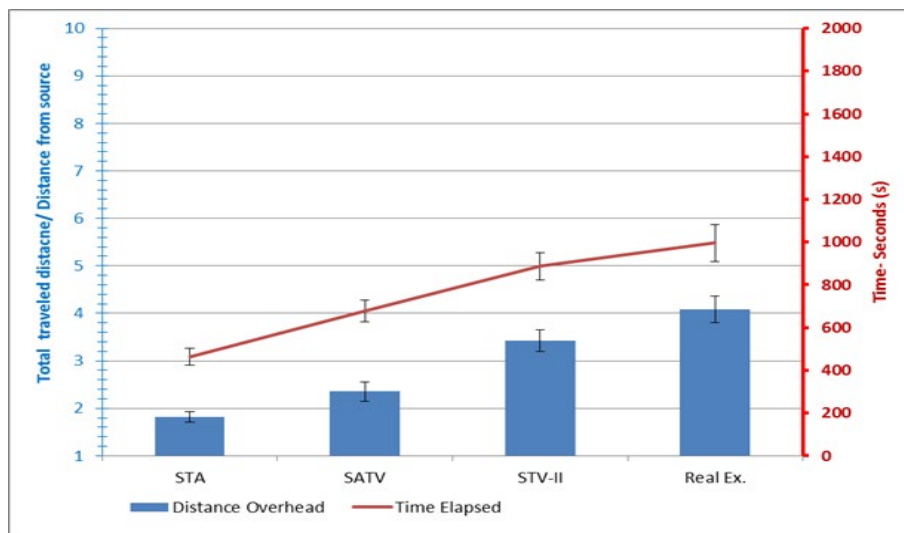


Fig. 31. The CPT performance of simulation models of STV-II, SATV, STA and real-experiment

## 5.0 CONCLUSIONS

In this study, we developed a CPT robot simulator with quadrotor platform and implemented a modified Gaussian-meandering plume propagation enhanced with the realistic characteristics of plume propagation such as meandering, internal intermittency, and vortices. This model was integrated with an open-source CFD software, TYCHO, to simulate the realistic effect of the environment windbreaks (with obstacles) on the chemical plume propagation. We also modelled the impact of a quadrotor’s propellers during CPT. Lastly, we find out that STV-II model has closer results to real-world which is under the controlled environment (the indoor experiment as shown in Fig 29). The limitations of this project are that we are not able to validate that the exacts propagation of these proposed models because it is only can be proved by using a wind tunnel. In addition, changes in the parameters of the experiment environment (such as outdoor environment, different filament dispersion rates, different wind speeds and dynamically changes in turbulent wind direction) have not been validated in this project. For future work, we will use a wind tunnel to validate our proposed models and also testing with different parameters of experiment environments. Furthermore, we will also consider a more realistic environment such as outdoor experiment, time-variant wind flows, and dynamics obstacles that can influence wind vectors.

## REFERENCES

- [1] M. McGrath, "California methane leak 'largest in US history,'" *BBC News*, 2016. [Online]. Available: <http://www.bbc.com/news/science-environment-35659947>. [Accessed: 31-Mar-2018].
- [2] A. K. Werner, S. Vink, K. Watt, and P. Jagals, "Environmental health impacts of unconventional natural gas development: A review of the current strength of evidence," *Sci. Total Environ.*, vol. 505, no. x, pp. 1127–1141, 2015.
- [3] A. Shukla and H. Karki, "Application of robotics in onshore oil and gas industry—A review Part I.," *Auton. Syst.*, vol. 75, pp. 490–507, 2016.
- [4] P. P. Neumann, B. V. Hernandez, A. J. Lilienthal, M. Bartholmai, and J. H. Schiller, "Gas source localization with a micro-drone using bio-inspired and particle filter-based algorithms," *Adv. Robot.*, vol. 27, no. 9, pp. 725–738, 2013.
- [5] K. Kurotsuchi, M. Tai, and H. Takahashi, "Vision-based Autonomous Micro-Air-Vehicle Control for Odor Source Localization," in *2016 23rd International Conference on Mechatronics and Machine Vision in Practice (M2VIP)*, 2016.
- [6] K. S. Eu, K. M. Yap, and T. H. Tee, "An Airflow Analysis Study of Quadrotor Based Flying Sniffer Robot," *Adv. Dev. Ind. Appl. Mech.*, vol. 627, pp. 246–250, 2014.
- [7] A. Marjovi and L. Marques, "Multi-robot odor distribution mapping in realistic time-variant conditions," in *Proceedings - IEEE International Conference on Robotics and Automation*, 2014, pp. 3720–3727.
- [8] J. P. Crimaldi, M. B. Wiley, and J. R. Koseff, "The relationship between mean and instantaneous structure in turbulent passive scalar plumes," *J. Turbul.*, vol. 5248, no. June 2001, pp. 27–29, 2002.
- [9] W. Jatmiko, Y. Ikemoto, T. Matsuno, T. Fukuda, and K. Sekiyama, "Distributed Odor Source Localization in Dynamic Environment," *IEEE Sensors, 2005.*, pp. 254–257, 2005.
- [10] J. A. Farrel, J. Murlis, X. Z. Long, W. E. I. Li, R. T. Carde, J. a Y. a Farrel, J. Murlis, X. Z. Long, W. E. I. Li, and R. T. Cardé, "Filament-Based Atmospheric Dispersion Model to Achieve Short Time-Scale Structure of Odor Plumes," *Environ. Fluid Mech.*, vol. 2, no. 1, pp. 143–169, 2002.
- [11] Z. Liu and T.-F. Lu, "A Simulation Framework for Plume-Tracing Research," *Australas. Conf. Robot. Autom.*, no. December, pp. 3–5, 2005.
- [12] B. L. Villarreal, G. Olague, and J. L. Gordillo, "Synthesis of Odor Tracking Algorithms with Genetic Programming," *Neurocomput.*, vol. 175, no. PB, pp. 1019–1032, Jan. 2016.
- [13] G. Ferri, M. V. Jakuba, A. Mondini, V. Mattoli, B. Mazzolai, D. R. Yoerger, and P. Dario, "Mapping multiple gas/odor sources in an uncontrolled indoor environment using a Bayesian occupancy grid mapping based method," *Rob. Auton. Syst.*, vol. 59, no. 11, pp. 988–1000, Nov. 2011.
- [14] A. Lilienthal and T. Duckett, "Building gas concentration gridmaps with a mobile robot," *Rob. Auton. Syst.*, vol. 48, no. 1, pp. 3–16, Aug. 2004.
- [15] Y. Wada, M. Trincavelli, Y. Fukazawa, and H. Ishida, "Collecting a Database for Studying Gas Distribution Mapping and Gas Source Localization with Mobile Robots," in *In Proceedings of the 5th International Conference on Advanced Mechatronic (ICAM)*, 2010, pp. 183–188.
- [16] A. T. Hayes, a. Martinoli, and R. M. Goodman, "Distributed odor source localization," *IEEE Sens. J.*, vol. 2, no. 3, pp. 260–271, Jun. 2002.
- [17] G. Cabrita, P. Sousa, and L. Marques, "PlumeSim-Player/Stage Plume Simulator," in *ICRA Workshop on Networked and Mobile Robot Olfaction in Natural, Dynamic Environments*, 2010.
- [18] A. Khaliq, "Gas Dispersal Simulation in ROS," Orebro University, 2011.
- [19] J. G. Monroy, J.-L. Blanco, and J. González-Jiménez, "An Open Source Framework for Simulating Mobile Robotics Olfaction," in *15th International Symposium on Olfaction and Electronic Nose (ISOEN)*, 2013, pp. 2–3.

- [20] B. Luo, Q. H. Meng, J. Y. Wang, and S. G. Ma, "Simulate the aerodynamic olfactory effects of gas-sensitive UAVs: A numerical model and its parallel implementation," *Adv. Eng. Softw.*, vol. 102, pp. 123–133, 2016.
- [21] J. Monroy, V. Hernandez-Bennets, H. Fan, A. Lilienthal, and J. Gonzalez-Jimenez, "GADEN: A 3D Gas Dispersion Simulator for Mobile Robot Olfaction in Realistic Environments," *Sensors*, vol. 17, no. 7, pp. 1–16, 2017.
- [22] M. F. E. Rohmer S. P. N. Singh, E. Rohmer, S. P. N. Singh, and M. Freese, "V-REP: a Versatile and Scalable Robot Simulation Framework," in *Proc. of The International Conference on Intelligent Robots and Systems (IROS)*, 2013, pp. 0–5.
- [23] M. R. Beychok, *Fundamentals of Stack Gas Dispersion*, 3rd Ed. Irvine, CA: Milton Beychok Pub, 1995.
- [24] N. S. Holmes and L. Morawska, "A review of dispersion modelling and its application to the dispersion of particles: an overview of different dispersion models available," *Atmos. Environ.*, no. 40, pp. 5902–5928, 2006.
- [25] Á. Leel'ossy, F. Molnár, F. Izsák, Á. Havasi, I. Lagzi, and R. Mészáros, "Dispersion modeling of air pollutants in the atmosphere: A review," *Cent. Eur. J. Geosci*, no. 6, pp. 257–278, 2014.
- [26] F. Gifford, "Statistical Properties of A Fluctuating Plume Dispersion Model," *Adv. Geophys.*, vol. 6, no. C, pp. 117–137, 1959.
- [27] P. Mussio, A. W. Gnyp, and P. F. Henshaw, "A fluctuating plume dispersion model for the prediction of odour-impact frequencies from continuous stationary sources," *Atmos. Environ.*, vol. 35, no. 16, pp. 2955–2962, 2001.
- [28] E. Yee and D. J. Wilson, "A comparison of the detailed structure in dispersing tracer plumes measured in grid-generated turbulence with a meandering plume model incorporating internal fluctuations," *Boundary-Layer Meteorol.*, vol. 94, no. 2, pp. 253–296, 2000.
- [29] E. Yee, R. Chan, P. R. Kosteniuk, G. M. Chandler, C. A. Biltoft, and J. F. Bowers, "Incorporation of internal fluctuations in a meandering plume model of concentration fluctuations," *Boundary-Layer Meteorol.*, vol. 67, no. 1–2, pp. 11–39, 1994.
- [30] H. Peterson and B. Lamb, "Comparison of results from a Meandering-Plume Model with measured atmospheric tracer concentration fluctuations," *Journal of Applied Meteorology*, vol. 31, pp. 553–564, 1992.
- [31] N. Ben Salem, P. Salizzoni, and L. Soulhac, "Estimating accidental pollutant releases in the built environment from turbulent concentration signals," *Atmos. Environ.*, vol. 148, pp. 266–281, 2017.
- [32] M. a R. Koehl, "The fluid mechanics of arthropod sniffing in turbulent odor plumes.," *Chem. Senses*, vol. 31, no. 2, pp. 93–105, Feb. 2006.
- [33] K. Karydis and V. Kumar, "Energetics in robotic flight at small scales," *Interface Focus*, vol. 7, no. 1, p. 20160088, 2017.
- [34] K. S. Eu, K. M. Yap, and W. C. Tan, "A Simulation Study of Micro-Drone Chemical Plume Tracking Performance in Tree Farm Environments," in *Advances in Visual Informatics*, vol. 8034, 2017, pp. 260–269.
- [35] W. Kapferer, "Tycho-CFD (Tyrolean Computational Hydrodynamics)," 2013. [Online]. Available: <http://www.tycho-cfd.at/>. [Accessed: 15-Nov-2017].
- [36] C. P. and W. Paul R., "The Piecewise Parabolic Method (PPM) for Gas-Dynamical Simulations," *J. Comput. Phys.*, vol. 54, pp. 174–201, 1984.
- [37] J. Gonzalez-Jimenez, J. G. Monroy, and J. L. Blanco, "The Multi-Chamber Electronic Nose--an improved olfaction sensor for mobile robotics.," *Sensors (Basel)*, vol. 11, no. 6, pp. 6145–64, Jan. 2011.
- [38] A. J. Lilienthal, A. Loutfi, and T. Duckett, "Airborne Chemical Sensing with Mobile Robots," *Sensors*, vol. 6, no. 11, pp. 1616–1678, Nov. 2006.
- [39] K. J. Albert and N. S. Lewis, "Cross Reactive Chemical Sensor Arrays," *Chem. Rev.*, no. 100, pp. 2595–2626, 2000.

- [40] K. S. Eu and K. M. Yap, "An Exploratory Study of Quadrotor's Propellers Impact Using 3D Gas Dispersion Simulator," in *The International Symposium on Olfaction and Electronic Nose (ISOEN)*, 2017.
- [41] A. Khaliq, S. Pashami, E. Schaffernicht, A. Lilienthal, and V. H. Bennetts, "Bringing Artificial Olfaction and Mobile Robotics Closer Together – An Integrated 3D Gas Dispersion Simulator in ROS," *16th Int. Symp. Electron. Noses*, p. 78, 2015.
- [42] K. S. Eu and K. M. Yap, "Chemical plume tracing: A three-dimensional technique for quadrotors by considering the altitude control of the robot in the casting stage," *Int. J. Adv. Robot. Syst.*, vol. 15, no. 1, 2018.